Defence Science Journal, Vol. 71, No. 5, September 2021, pp. 662-669, DOI : 10.14429/dsj.71.16398

Investigations on Monolithic Radome Interactions with Active Electronically Scanned Array on Fighter Platform

Akumalla Lakshmaiah[#,*], N.N.S.S.R.K. Prasad[#], and K.P. Ray[@]

[#]*DRDO-Aeronautical Development Agency, Bengaluru - 560 017, India*
[@]*DRDO-Defence Institute of Advanced Technology, Pune - 411 025, India*
[*]*E-mail: lakshmaiah@jetmail.ada.gov.in*

ABSTRACT

The conventional fighter aircrafts are often equipped with fire control radar (FCR) using mechanically scanned antenna (MSA) with passive slots enclosed with monolithic conical radome. When the fighter platforms get upgraded with the modern active electronically steered array (AESA) FCR for better mission capabilities, even though radome change is desirable for optimum performance of AESA, it may not be feasible due to development time. This necessitate the evaluation of AESA radar with the existing monolithic radome. Hence active antenna aperture radiation pattern is required to be assessed with monolithic radome. To address this issue, simulation is preferred over physical testing, due to the reduced cost, time and complexity in measurements and ability to verify compatibility. In the present paper, the influence of monolithic radome on the active antenna radiation patterns are simulated and analysed. The characterisation studies helped for better optimisation of active aperture, optimum size for new radome development and additional space on fighter platforms that can be used for integration of new sub-systems. Simulations are performed at two different locations of antenna inside radome. Experimental validations have been carried out to prove the efficacy of simulated results, which are in agreement.

Keywords: Fire control radar; Active electronically scanned array; Monolithic radome; Variable thickness radome

1. INTRODUCTION

The fire control radar (FCR) uses mechanically scanned antenna (MSA) with passive slotted array that has limited capabilities in providing situational awareness and advanced mission features for fighter aircraft. As per the modern day requirements, many fighter platforms are upgrading with modern active electronically steered array (AESA) radar that brings an advantage of enhanced situation awareness and wide frequency band coverage. In case of passive antenna radar, the antenna is positioned at different look angles by an electronic position controller. Whereas, in AESA radar, the antenna is actively controlled; the beam is steered at different look angles by controlling the phase of each antenna element in the array[1]. In fighter aircrafts, the FCRs are enclosed by nosecone. The nosecone is shaped as per the aircraft aerodynamics, structural requirements. Also to provide an environmental protection as radome with maximum Electromagnetic (EM) transparency. Despite of the structural characteristics, the EM properties of radome are most essential for the optimum behaviour of FCR.

The close proximity of radome to the antenna affects its radiation pattern and leads to the attenuation of radiated energy, causes antenna principal beam deflection from the expected bore sight and degrades side lobe levels (SLLs). These arguments are quantified as EM performance of radome in terms of transmission efficiency, boresight error (BSE) and SLL degradation[1-6]. The transmission efficiency and SLLs will have impact on radar detection capabilities and BSE on the tracking accuracies[7-11]. The BSE can be measured and corrected in the beam position in FCR. These parameters are mainly depending on the dielectric characteristics of material, shape and wall thickness of the radome. The dielectric properties play a major role for transmission efficiency and BSE. The shape and wall thickness are essential for structural stability.

The EM characteristics of radome are strongly related to the aperture and location of the antenna with respect to radome wall as radome is in the near field of antenna much before main beam formation. With the mechanically scanned arrays, separation between the antenna and radome wall is always required to enable the scan movements of the antenna at different look angles[12-18]. However, with AESA, the antenna can even be kept at very near to the radome wall with minimum separation required for mechanical accessibility. This approach has its own benefits as it creates more internal space in the aircraft which can be utilised for integration of additional tactical sensors to enhance the mission capabilities. However, the assessment of EM performance is also required to be considered in deciding the minimum separation with radome inner wall and antenna. An EM characterisation study of the radome is critical in deciding the tradeoff.

Received : 14 October 2020, Revised : 08 February 2021
Accepted : 18 February 2021, Online published : 02 September 2021

So far the design studies and analysis were carried out for various types and sizes of radome with passive antenna array, which have reciprocal, symmetrical radiation patterns at one specific location inside radome. The AESA radiation patterns are generally non-symmetrical and non-reciprocal. Previously very limited studies are reported on effects of radome on the active array radiation patterns[19-23]. Studies have been carried out to understand the electrical performance of A-sandwich radome by strip loading[24.] A thick FSS radome wall has been proposed for airborne application based on mode-matching generalised scattering matrix approach[25].

In our previous work, studies on nosecone radome effects of AESA Radar have been presented briefly[26]. In the present work, the investigations of radome effects on the radiation pattern of active array antenna is done at two different locations of antenna inside radome.

(i) 200 mm (typical separation between radome base and antenna aperture).
(ii) 450 mm (Aperture at much way from the radome base and minimum distance from the radome wall) from the radome base.

In the first approach, one location is taken by considering the conventional separation of around four wavelengths between antenna elements at the outer edge and the closest radome wall. In second approach, the separation is reduced to less than a wavelength, so that the radome wall is within the near field boundary of outer elements. The actual AESA aperture and the existing monolithic radome of fighter aircraft are used for the studies.

Hybrid techniques were proposed[27-30] to solve the electrically large radomes. The effect of radome on active array radiation patterns is simulated and quantified in terms of transmission efficiency and side lobe levels using the full wave simulations with the help of commercially available FEKO EM simulation tool[31]. These simulation results are verified with measurements of monolithic radome. The results of the analysis helped in design optimisation of AESA aperture, reduction in radome size and space optimisation for integration of new systems, for futuristic fighter aircraft requirements.

2. ANTENNA AND RADOME MODELS FOR SIMULATIONS

2.1 Antenna Model

An active antenna aperture is designed using trans/receive (T/R) modules with solid state amplifiers of semiconductors like Gallium Arsenide (GaAs) or Gallium Nitrate (GaN). Each antenna element is integrated with T/R module to facilitate transmit and receive operations, the antenna elements are printed dipoles designed for wide bandwidth applications. The number of antenna elements and its inter element spacing are the key factors to achieve required effective antenna aperture. The usage of T/R module provides flexibility in the formation of desired beam patterns. In this work, an antenna model is constructed using about 712 wire dipoles in X-band. The elements arrangement is in quasi circular form to achieve better side lobe levels in comparison with rectangular and circular arrangements. The full wave solution using Multilevel Fast Multipole Method (MLFMM) is used to achieve better accuracy while reducing computational resources. The optimum mesh size is greater than $\lambda/7$ and the selected mesh size is $\lambda/12$.

2.2 Radome Model

Various types of radome configurations like monolithic, sandwich and FSS designs are used based on the applications and type of radar it hosts. A monolithic radome wall configuration using quartz material with relative permittivity $\varepsilon_r = 3.5$ and a loss tangent $\tan\delta = 0.005$ is considered in this work. The length and base diameter of the radome is 2000 mm and 900 mm respectively with thickness (*d*) 9.0 mm at the non critical zone. The Antenna enclosed with monolithic conical radome model is illustrated in Fig. 1(a). The nosecone radome is fitted with metallic probe, lightning strip and air data pneumatic pipes. The nose cone on fighter platform is installed typically with a depression angle of 6° for the visual clearance. Due to this, radome is symmetrical about Antenna azimuth axis only. So the effects of radome on antenna patterns in azimuth axis are emphasised.

The wall thickness of monolithic radome, *d,* can be determined from Eqn (1)[31]:

$$d = \frac{m\lambda}{2}\sqrt{\varepsilon - \sin^2\theta} \tag{1}$$

where λ is the operating wavelength, θ is incident angle, ε is the dielectric constant of the substrate material used and *m* is an integer.

The transmission and reflection loss of a radome wall with thickness *d,* can be computed with the help of Eqn (2)

$$R = 2j\Gamma \sin D/\psi \tag{2a}$$

$$T = (1-\Gamma^2)/D \tag{2b}$$

where $D = (1-\Gamma^2)\cos\psi + j = (1+\Gamma^2)\sin\psi$

and $\psi = kd\sqrt{\varepsilon - \sin^2\theta}$

Γ is the reflection coefficient which can be given as:

$$\Gamma = \left(\frac{y_1 - y_2}{y_1 + y_2}\right) \tag{3a}$$

In which y_1 is the air admittance:

$$y_1 = \begin{cases} \cos\theta & TE \\ 1/\cos\theta & TM \end{cases} \tag{3b}$$

And y_2 is the dielectric substrate admittance:

$$y_2 = \begin{cases} \sqrt{\varepsilon - \sin^2\theta} & TE \\ \varepsilon/\sqrt{\varepsilon - \sin^2\theta} & TM \end{cases} \tag{3c}$$

The above equations can be helpful for computing the transmission response of the radome wall.

In general, variable thickness radomes (VTR) are preferred over the constant thickness radome (CTR) designs for streamlined airborne applications and to make the tradeoff between transmission efficiency and boresight

error[6]. The transmission characteristics for both TE, TM configurations at various incident angles are given in Fig. 1(b) and Fig. 1(c) respectively at the wall thickness of 9.0 mm. It is observed that the transmission loss at operating band is less than 0.6 dB and increased at higher incident angle for TE polarisation. Similarly, for TM polarisation the loss is reduced at higher incident angle.

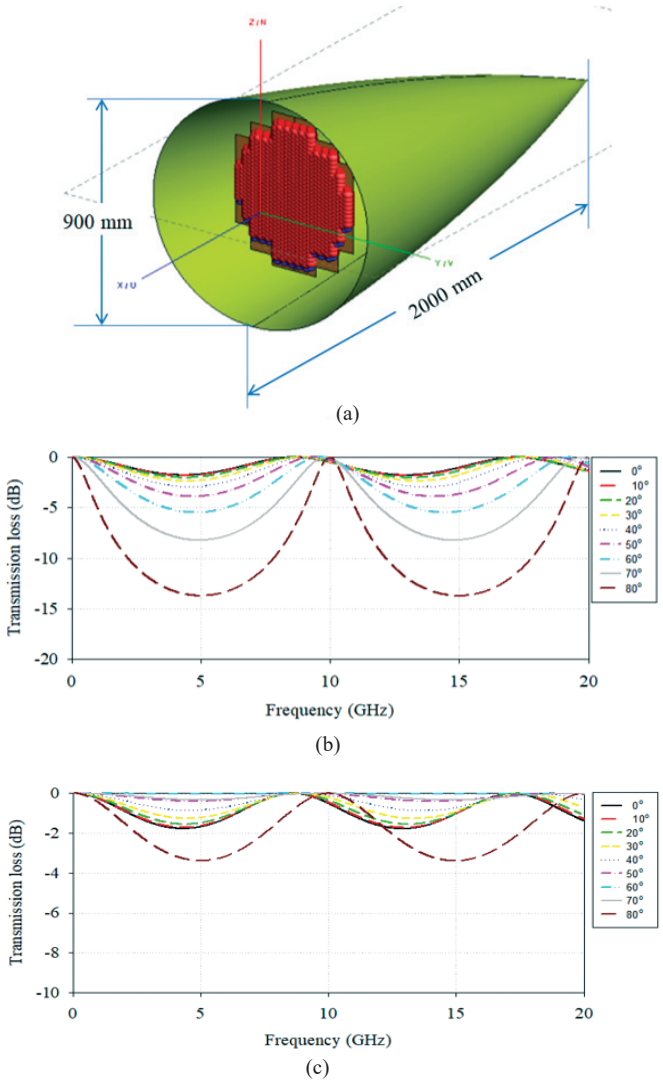

Figure 1. (a) Radome enclosed antenna, (b) Transmission characteristics at oblique incident angles for TE, and (c) Transmission characteristics at oblique incident angles for TM.

3. RADOME ON ANTENNA RADIATION PATTERN

AESA radars provide the degree of flexibility in the formation of beam patterns. Due to non reciprocal pattern formation, AESA uses uniform distribution during transmission and non uniform distribution during reception. The uniform distribution provides an advantage of additional gain for the radar performance, whereas non-uniform (tapered) distribution provides the advantage of reduced side lobe level. The requirement to have minimal effect to AESA FCR performance over the wide band with the two different amplitude distributions makes the EM design of radome more complex. The analysis of AESA and radome has been performed in the operating frequency (f_2) in X – band at 10 GHz.

3.1 Radome Effect on Uniform Amplitude Distribution

Equal amplitude is applied for all the dipole elements of antenna to generate uniform distribution pattern. The normalised uniform radiation pattern of antenna with and without radome is shown in Fig. 2(a). It is observed that the main lobe is attenuated due to the presence of radome and also the side lobes have degraded (increased) by around 10 dB at 30° from the bore sight axis. This is mainly due to loss and reflections at higher incident angles. The first side lobe level is observed about 20 dB down as expected due to quasi circular distribution of Antenna elements.

3.2 Radome Effect on Non-uniform Amplitude Distribution

The non-uniform radiation distribution is obtained by applying Taylor's n line distribution[19]. As expected the first SLL of antenna pattern is 30 dB down and the gain is reduced and beam width is increased in this distribution as shown in Fig. 2(b). It is observed that the presence of radome has degraded the SLL about 5 dB for first side lobe and up to

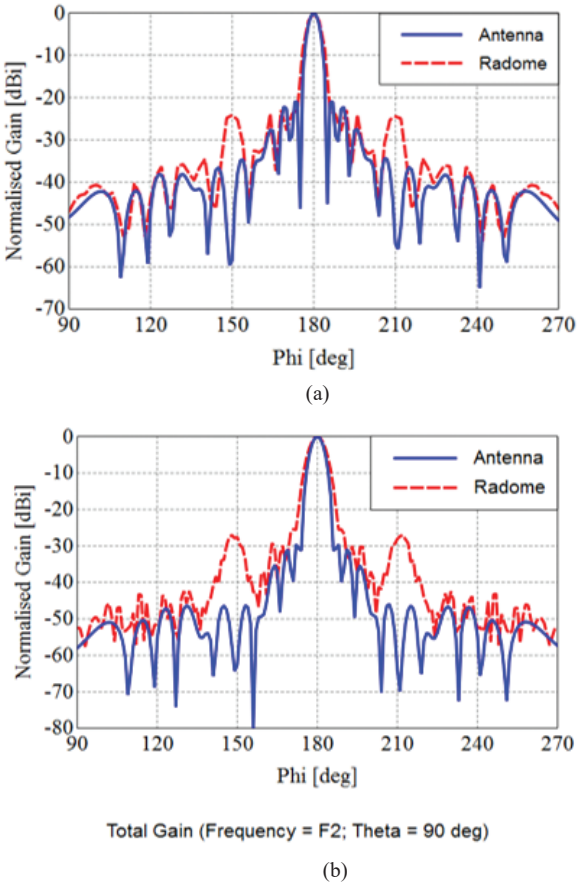

Figure 2. Radiation pattern of antenna and radome enclosed antenna at boresight axis: (a) uniform amplitude distribution and (b) non-uniform amplitude distribution.

25 dB at 30° from the bore sight axis that is almost equal to first side lobe level. This indicates the necessity to optimise the thickness profile of new radome design for better control of SLL of AESA. The BSE of radome is essential for target tracking of FCR. As per the studies the radome design is trade-off between transmission efficiency and BSE. So the design goal is to emphasise optimum transmission efficiency as the BSE needs to be measured and can be corrected in FCR.

3.3 Comparison of Radome Effect on Antenna Radiation Pattern Distribution

The radiation pattern of uniform and amplitude (non-uniform) distribution of radome enclosed antenna is shown in Fig. 3(a). The error plot of uniform and non-uniform pattern with radome enclosed antenna is shown in Fig. 3(b). It is observed that the radome effect on pattern distribution in terms of loss is about 0.28 dB and in terms of SLL is about 5 to 10 dB in amplitude distribution. So the radome design optimisation is essential for amplitude distribution pattern in the case of AESA enclosed radome.

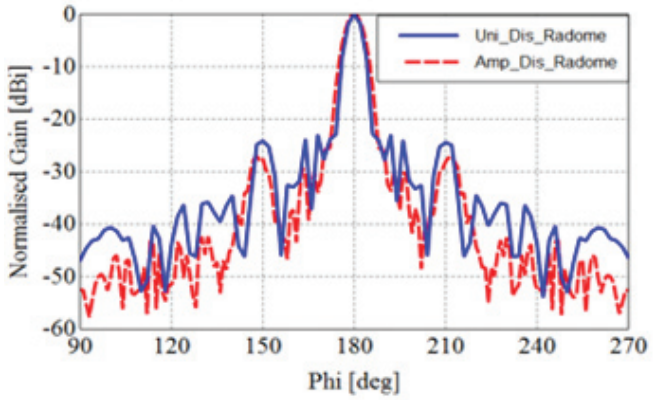

Figure 3. (a) Radiation pattern of uniform and non-uniform amplitude distribution with radome at bore sight axis and (b) Error between uniform and non-uniform amplitude distribution.

3.4 Effect of Radome at Off Boresight Angles

In the fighter platform, the FCR performance is an unavoidable performance characteristic. To understand this phenomenon, simulations are carried out to study the effect of radome on non–uniform distribution patterns at different look angles with 10° step from 0° to 60° on one side of the radome in azimuth plane. The radiation patterns of antenna and radome enclosed antenna for look angles at 30° and 60° are shown in the Fig. 4(a) and Fig. 4(b) respectively. It is observed that the AESA radiation pattern is non symmetric for the look angles at off bore sight unlike passive array. As expected the gain is reduced and beam width is increased at off bore sight angles, the SLLs are asymmetrical due to variation in array element gain and reduction in active aperture at off boresight angles. So it is essential for radome design to focus on asymmetric side lobe levels.

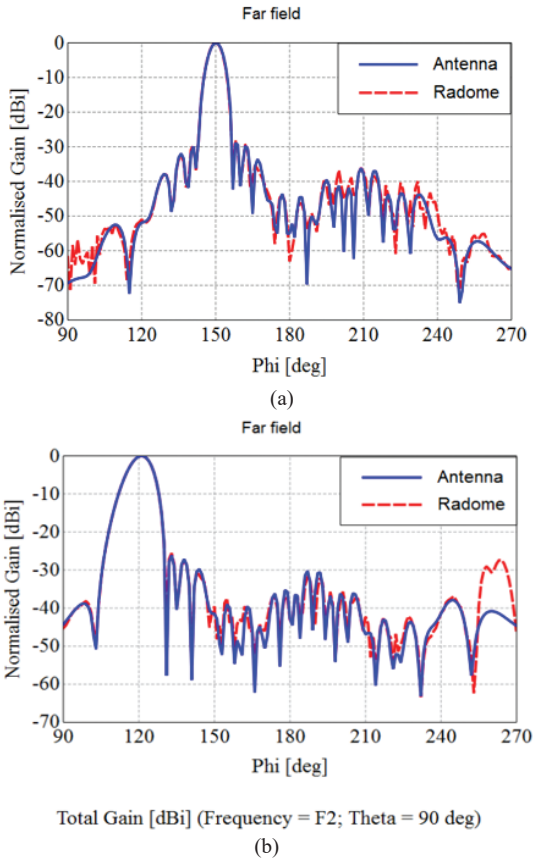

Figure 4. Radiation pattern of antenna and radome with non-uniform amplitude distribution: (a) -30° look angle and (b) -60° look angle.

4. RELOCATION OF ANTENNA INSIDE RADOME

The new fighter variants are to be developed to cater for additional mission capabilities, which demands modern sensors. As the onboard equipments are tightly packed within a limited space any additional space is an extremely demanded resource. The Infrared Search and Track (IRST) systems and retractable midair refuelling system are two major systems in the advanced fighter aircrafts. These two systems are mandatorily to be located in the front section of the fighter platform to have

clear vision in the forward direction. A technique is attempted to optimise the separation between radome and antenna by shifting the antenna forward to create additional space for these systems.

The conventional passive array is installed at about 200 mm from radome base with sufficient gap between antenna and inner wall of radome of about 4λ to facilitate MSA rotations as shown in Fig. 5(a). However, in the case of AESA, the scan volume is attained by steering the beam electronically using phase shifters without mechanical rotations. So, based on optimum installation and removal requirements of radome, the gap is reduced to less than 1λ by shifting AESA from radome base of about 450mm inside radome as shown in the Fig. 5(b).

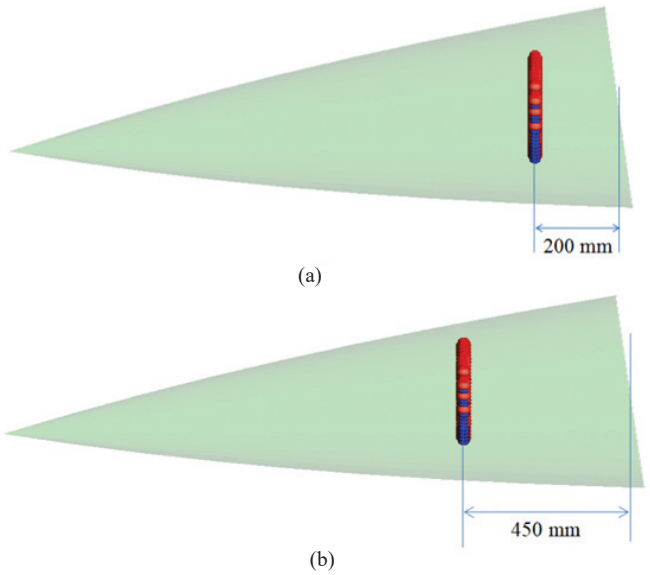

Figure 5. Representation of AESA antenna inside radome: (a) 200 mm, (b) 450 mm.

The effect of radome on antenna at new location is studied in this section. The radiation patterns at look angles of 0°, 30° and 60° at initial and shifted locations are shown in Figs. 6(a), 6(b), and 6(c) respectively. The relationship between radar range and TL is derived from radar range Eqn (4)[20]. Assuming one-way TL and other parameters remains the same in the above equation, the difference in one-way TL of 0.15 dB will have reduction of approximately <2% in range. The effect of radome on antenna relocation at three look angles is found to be minimal, on first side lobe and near side lobe levels and less than 2 dB at far side lobes.

$$R_2 = R_1 \left(10^{-2(TL/10)}\right)^{\frac{1}{4}} \quad (4)$$

In the above expression, R_1 and R_2 are estimated radar ranges at initial and shifted locations of AESA inside the radome.

This comparison provides the confidence in changing the location of the antenna with this approach, it is also feasible to integrate new sensors and also upgrade existing fighter to new configuration by reducing the size of the radome with appropriate mechanical process.

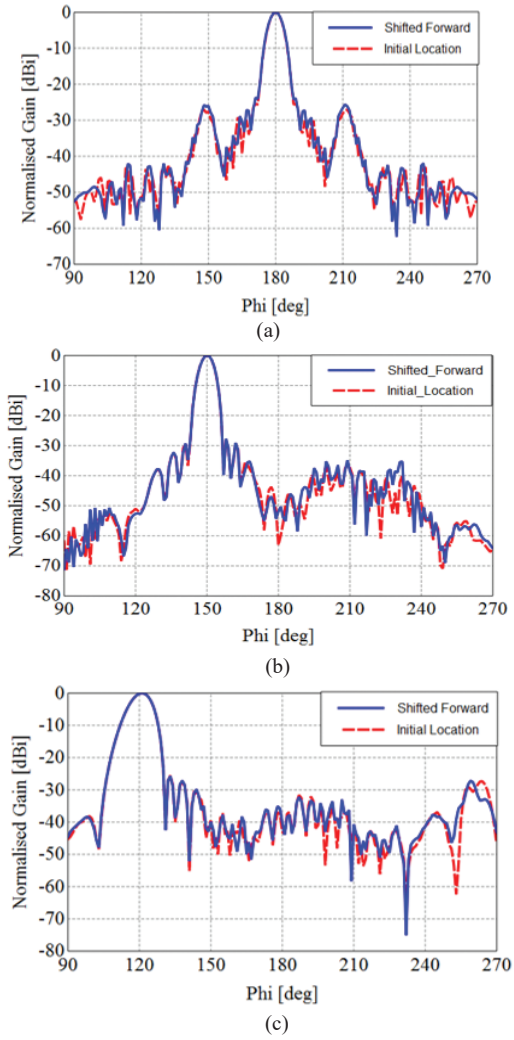

Figure 6. Comparison of radiation patterns of radome at 30° off bore sight with array at initial location and forward location: (a) 0°, (b) 30°, and (c) 60°.

5. RESULTS AND DISCUSSION

A standard experimental set up consisting of actual radar antenna enclosed with monolithic radome is used for measuring the transmission loss. As the radome is symmetrical along x – and y – axis, the loss is same on either sides of the radome axis. The transmission loss across the look angles in azimuth axis is measured. It is observed that the maximum TL is at 0° look angle due to the high incident angle of the antenna to the normal axis of radome wall and reduced at off boresight angles from 0° to 60°. The EM measurement of radome with actual AESA antenna is a complex task. A dedicated test setup is required to be developed for such task. It requires beam formation and steering with power and cooling system. This is costly and time consuming effort. So the simulation results are analysed with actual measurements of radome that were carried out with existing MSA. The TL measurement was carried out at every 0.5° from -60° to +60° in azimuth axis. The radome TL comparison of simulated results at initial and forward location with AESA along with measured MSA results is shown in Fig. 7. It is observed form the simulated results that the trend of TL along the azimuth axis is close to

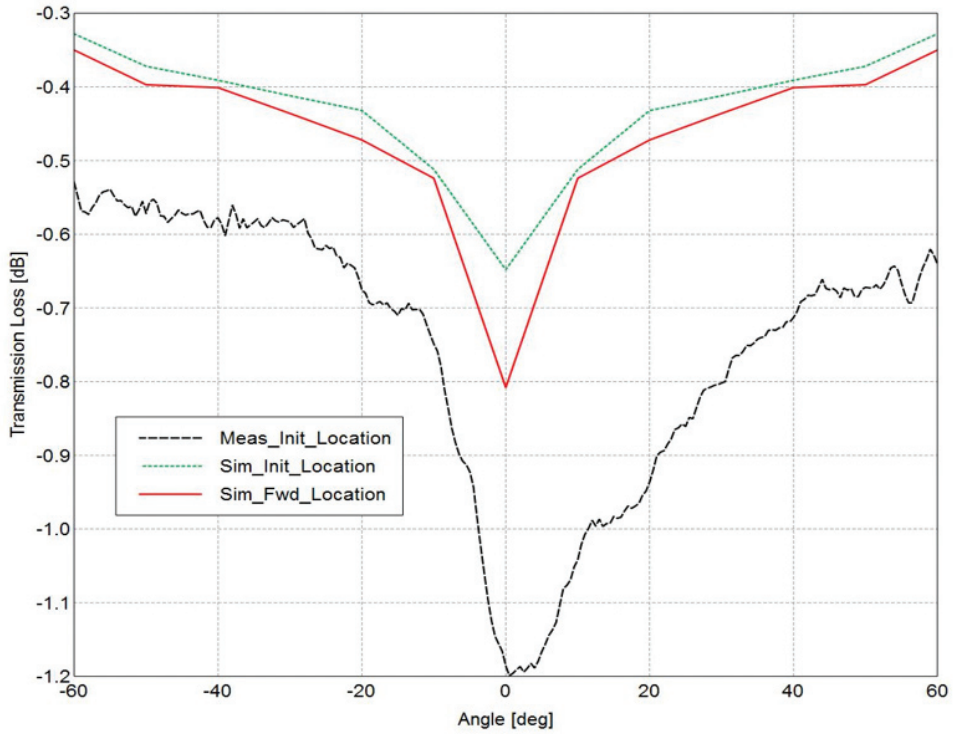

Figure 7. Radome transmission loss comparison between measured and simulated results at initial (200 mm) and forward location (450 mm).

each other at both initial and forward locations. Maximum of 0.15 dB difference at boresight and less than 0.1 dB at all other angles is observed. It is observed from the measured data that the maximum loss is at boresight i.e. 0° look angle and reduced at off boresight angles. The trend of transmission loss between simulations and measurements is almost similar. The non symmetrical phenomena in the TL of measured data is due to additional lightning strip on right side (positive angles) and the sharp rise of around 0.55 dB between 0° to 15° is due to metallic probe and pneumatic pipes of the radome used for the measurements. Hence, the radome performance in general is classified into different zones[32]. For better radar performance, such metallic probe and pneumatic pipes needs to be avoided with alternate suitable arrangements for air data in new fighter aircrafts.

6. CONCLUSIONS

The analysis and rigorous study has been conducted on the radome interactions with antenna at two different locations for various look angles inside the radome. From the obtained results. It is determined that the effect of radome on antenna due to forward shift towards the nose tip is minor. The effect on FCR performance is negligible in comparison to the advantage of enhanced fighter platform capabilities in terms of additional space for new sensor system integration, optimisation of antenna aperture, reduction in radome length and fabrication cost.

REFERENCES

1. Christopher, S.; Active Electronically-steered Array Surveillance Radar: Indian Value Addition. *Def. Sci.J.*, 2010, **60**(2), 184-188. doi: 10.14429/dsj.60.338
2. Kozakoff, D. J. Analysis of radome-enclosed antennas. Second edition, Artech Huose, 685, Canton Street, Norwood, MA 02062 USA, 2010
3. Rotgerink, J. L; Van der Ven, H.; Voigt, T.; Jehamy, E.; Schick, M. & Schippers, H. Modelling of effects of nose radomes on radar antenna performance. *10th European Conference on Antennas and Propagation (EuCAP)*, Davos, 2016, pp. 1-5. doi: 10.1109/EuCAP.2016.7481773
4. Yazeen, P. S. M.; Vinisha, C. V.; Vandana, S.; Suprava, M. & Nair, R. U. Electromagnetic Performance Analysis of Graded Dielectric Inhomogeneous Streamlined Airborne Radome. *IEEE Transactions on Antennas and Propagation*, 2017, **65**(5), 2718-2723.
5. Sukharevsky, O.; Vasylets, V. & Nechitaylo, S. Scattering and radiation characteristics of antenna systems under nose dielectric radomes. *Progress in Electromagnetics Research B*, 2017, **76**, 141-157. doi: 10.2528/PIERB17032208
6. Zhao, W, -J.; Gan, Y, -B.; Wang, C, -F, & Li, L, -W. Radiation pattern and input impedance of a radome-enclosed planar dipole array backed by a ground plane. *IEEE Antennas and Propagation Society International Symposium*, Washington, DC, 2005, **1A**, 350-353. doi: 10.1109/APS.2005.1551322
7. Nair, R. U. & Jha, R. M. Electromagnetic Performance Analysis of a Novel Monolithic Radome for Airborne Applications. *IEEE Transactions on Antennas and Propagation*, 2009, **57**(11), 3664-3668. doi: 10.1109/TAP.2009.2026595
8. Siwiak, K.; Dowling, T. & Lewis, L. Boresight errors

induced by missile radomes. *IEEE Transactions on Antennas and Propagation*, 1979, **27**(6), 832-841 doi: 10.1109/TAP.1979.1142193

9. Lee, H.-S. & Park, H. Prediction of Radome Bore-Sight Errors Using a Projected Image of Source Distributions. *Progress in Electromagnetics Research*, 2009, **92**, 181-194. doi: 10.2528/PIER09033105
10. Zhao, W.; Gan, Y.; Li, L. & Wang, C. Effects of an Electrically Large Airborne Radome on Radiation Patterns and Input Impedance of a Dipole Array. *IEEE Transactions on Antennas and Propagation*, 2007, **55**(8), 2399-2402. doi: 10.1109/TAP.2007.901916
11. Garcia, E.; Delgado, C.; Diego, I. G. & Catedra, M. F. An Iterative Solution for Electrically Large Problems Combining the Characteristic Basis Function Method and the Multilevel Fast Multipole Algorithm. *IEEE Transactions on Antennas and Propagation*, 2008, **56**(8), 2363-2371. doi: 10.1109/TAP.2008.926781
12. Crone, G. A. E.; Rudge, A. W. & Taylor, G. N. Design and performance of airborne radomes: A review. *IEE Proceedings F - Communications, Radar and Signal Processing*, 1981, **128**(7), 451-464, doi: 10.1049/ip-f-1.1981.0077
13. Richmond, J. Antenna pattern distortion by dielectric sheets. *IRE Transactions on Antennas and Propagation*, 1956, **4**(2), 139-142. doi: 10.1109/TAP.1956.1144381
14. Piche, A.; Piau, G.; Bernus, C.; Campagna, F. & Balitrand, D. Prediction by simulation of electromagnetic impact of radome on typical aircraft antenna. *The 8th European Conference on Antennas and Propagation (EuCAP 2014)*, The Hague, 2014, 3205-3208. doi: 10.1109/EuCAP.2014.6902510
15. KrushnaKanth, V. & Raghavan, S. Design and development of angularly stable and polarisation rotating FSS radome based on substrate-integrated waveguide technology. *IET Microwaves, Antennas & Propagation*, 2019, **13**(4), 478-484. doi: 10.1049/iet-map.2018.5386
16. Narayan, S.; Gulati, G.; Sangeetha, B. & Nair, R. U. Novel Metamaterial-Element-Based FSS for Airborne Radome Applications, *IEEE Transactions on Antennas and Propagation*, 2018, **66**(9), 4695-4707. doi: 10.1109/TAP.2018.2851365
17. Nair, R. U.; Suprava, M. & Jha, R. M. Graded dielectric inhomogeneous streamlined radome for airborne applications. *Electronics Letters*, 2015, **51**(11), 862-863. doi: 10.1049/el.2015.0462
18. Qamar, Z.; Aboserwal, N. & Salazar-Cerreno, J. L. An Accurate Method for Designing, Characterizing, and Testing a Multi-Layer Radome for mm-Wave Applications. *IEEE Access*, 2020, **8**, 23041-23053. doi: 10.1109/ACCESS.2020.2970544
19. Kedar, K.; Beenamole, S. & Revankar, U. K. Performance Appraisal of Active Phased Array Antenna in Presence of a Multilayer Flat Sandwich Radome. *Progress In Electromagnetics Research*, 2006, **66**, 157-171. doi:10.2528/PIER06111203
20. Skolnik, M. I. Non-uniform Arrays, R. E. Collin & F. J. Zucker(eds.), Ch. 6, 227–234, McGraw-Hill, New York, 1969.
21. Steinberg, B. D. Principles of Aperture and Array Systems Design, John Wiley and Sons, New York, 1976.
22. Miller, C. J. Minimizing the effects of phase quantization errors in an electronically scanned array. *Proc. 1964 Symp. Electronically Scanned Phased Arrays and Applications,* 1964, RADCTDR-64-225, RADC Griffiss AFB, 17–38.
23. Mailloux, R. J. Phased Array Antenna Handbook, Artech House,2005.
24. Narayan, S.; Nair, R, U. & Jha, R. M. Mode-matching Generalised Scattering Matrix Based Electromagnetics Performance Analysis of Thick Frequency Selective Surfaces for Airborne Applications. *Def. Sci. J.*, 2013, **63**(3), 249-253. doi:10.14429/dsj.63.2426
25. Nair, R.; Madhumitha, J. & Jha, R. M. Application of Metallic Strip Gratings for Enhancement of Electromagnetic Performance of A-sandwich Radome. *Def. Sci. J.*, 2013, **63**(5), 508-514. doi:10.14429/dsj.63.2458
26. Lakshmaiah, A.; Ray, K. P. & Prasad, NNSSRK. Analysis of Nosecone Radome Effects of Active Electronically Scanned Array(AESA) Radar Performance of Fighter Aircrafts. *IEEE Indian Conference on Antennas and Propogation (InCAP)*, 2019. doi: 10.1109/InCAP47789.2019.9134620
27. Hu, X.-W.; Xu, M. & Zheng, Y. More Accurate Hybrid PO-MoM Analysis for an Electrically Large Antenna-Radome Structure. *Progress In Electromagnetics Research*, 2009, **92**, 255-265. doi:10.2528/PIER09022301
28. Nie, X.-C.; Yuan, N.; Li, J. L.-W.; Yeo, T. S. & Gan, Y.-B. Fast Analysis of Electromagnetic Transmission through Arbitrarily Shaped Airborne Radomes Using Precorrected-FFT Method. *Progress In Electromagnetics Research*, 2005, **54**, 37-59, doi:10.2528/PIER04100601
29. Meng, H. F. & Dou, W.-B. A Hybrid Method for the Analysis of Radome-Enclosed Horn Antenna, Progress. *Electromagnetics Research*, 2009, **90**, 219-233. doi:10.2528/PIER08122502
30. Altair Engineering Inc., FEKO, Suite 7.0, 2014.
31. Benjamin Rulf & Gregory A. Robertshaw, Understanding the Antennas for Radar. Communication and Avionics. New York: Van Nostrand Reinhold Company Inc., 1987.
32. Prasad, NNSSRK,; Krishna, CHVRSG. & Kumar, D. Electromagnetic characterization of airborne radome of Fighter aircraft for Multimode Radar applications. *10th International Conference on Electromagnetic Interference & Compatibility*, Bangalore, 2008, 319-323.

ACKNOWLEDGEMENTS

Authors would like to acknowledge the encouragement and support received form PGD(CA) & Dir-ADA and TD(Av&WS). Sincere thanks to Mr D. Seshagiri, PD (UTTAM) and Mr G. Hemprasad, Sc 'E' of LRDE for providing technical guidance in antenna aperture simulations. Thanks are also due to Dr V. Krushna Kanth in revising the manuscript.

CONTRIBUTORS

Mr Akumalla Lakshmaiah received BTech (Electronics and Communication) from Jawaharlal Nehru Technological University, Ananthapur, India. He is working for Aeronautical Development Agency, Ministry of Defence. His area of research involves: Multimode airborne radar, Nose cone radome for fighter platform, Active Electronically Scanned array radar. He is currently pursuing MS at Defence Institute of Advanced Technology, DRDO, Pune, India.
In the current study, he simulated the radome and active array models and carried out analysis of results and proposed new concept for optimisation of antenna radome locations to create space for new sensors integration.

Dr N.N.S.S.R.K. Prasad received PhD (Electrical Engineering) from IIT- Bombay. He is presently working as Scientist/Engineer 'H' and Project Director (LCA AF Mk1A) & Assoc Technology Director (Avionics) in Aeronautical Development Agency (ADA) for LCA project. He has more than 100 publications in journals, conferences, and symposiums.
Contribution in the current study, he provided guidance for approach and statistical advice in execution of simulations and analysis. Also provided recommendation for implementation on futuristic fighter platform.

Dr K.P. Ray is PhD from Department of Electrical Engineering IIT, Bombay. Presently he is a Professor, Dean Research and head of the Department of Electronics Engineering, Defence Institute of Advanced Technology (DIAT), Pune. Prior to this he was a Programme Director of Society for Applied Microwave Electronics Engineering and Research (SAMEER) Mumbai, wherein he joined SAMEER (TIFR) in 1985 and worked in the areas of RF and microwave systems/components and developed expertise in the design of antenna elements/arrays and high power RF/microwave sources for RADAR and industrial applications. Has co-authored a book with Prof G. Kumar for Artech House, USA and published over 350 research papers in international/national journals and conference proceedings. He holds 3 patents and filed three patents. Has is an associate editor of many International Journals.
In the current study, he conceived the idea of the proposed optimisation of AESA and nose cone radome interactions, guided in analysis of results and approved the final result and manuscript.